Structure
Article

High-Speed Atomic Force Microscopic Observation of ATP-Dependent Rotation of the AAA+ Chaperone p97

Kentaro Noi,[1,2,7] Daisuke Yamamoto,[3,6,8] Shingo Nishikori,[1,6,9] Ken-ichi Arita-Morioka,[1,2] Takayuki Kato,[5] Toshio Ando,[3,4,6] and Teru Ogura[1,2,6,*]

[1]Department of Molecular Cell Biology, Institute of Molecular Embryology and Genetics
[2]The Global COE (Cell Fate Regulation Research and Education Unit)
Kumamoto University, Kumamoto 860-0811, Japan
[3]Department of Physics
[4]Bio-AFM Frontier Research Center
Kanazawa University, Kanazawa 920-1192, Japan
[5]Graduate School of Frontier Biosciences, Osaka University, Osaka 565-0871, Japan
[6]Core Research for Evolutional Science and Technology, Japan Science and Technology Agency, Tokyo 102-0075, Japan
[7]Present address: Department of Mechanical Science and Bioengineering, Graduate School of Engineering Science, Osaka University, Osaka 560-8531, Japan
[8]Present address: Department of Applied Physics, Fukuoka University, Fukuoka 814-0180, Japan
[9]Present address: Otsuka Pharmaceutical Co., Ltd., Tokushima 771-0192, Japan
*Correspondence: ogura@gpo.kumamoto-u.ac.jp
http://dx.doi.org/10.1016/j.str.2013.08.017

SUMMARY

p97 (also called VCP and CDC-48) is an AAA+ chaperone, which consists of a substrate/cofactor-binding N domain and two ATPase domains (D1 and D2), and forms a homo-hexameric ring. p97 plays crucial roles in a variety of cellular processes such as the ubiquitin-proteasome pathway, the endoplasmic reticulum-associated protein degradation, autophagy, and modulation of protein aggregates. Mutations in human p97 homolog VCP are linked to neurodegenerative diseases. The key mechanism of p97 in these various functions has been proposed to be the disassembly of protein complexes. To understand the molecular mechanism of p97, we studied the conformational changes of hexameric CDC-48.1, a *Caenorhabditis elegans* p97 homolog, using high-speed atomic force microscopy. In the presence of ATP, the N-D1 ring repeatedly rotates ~23 ± 8° clockwise and resets relative to the D2 ring. Mutational analysis reveals that this rotation is induced by ATP binding to the D2 domain.

INTRODUCTION

AAA+ (ATPases associated with diverse cellular activities) family proteins are ATP-dependent molecular chaperones, which exert mechanical work on macromolecular substrates, such as unfolding of proteins and disassembly of multisubunit protein complexes (Ogura and Wilkinson, 2001; Hanson and Whiteheart, 2005). It has been proposed that AAA+ chaperones undergo conformational changes during the cycle of ATP hydrolysis, and that the conformational changes provide their mechanical work on substrates. AAA+ proteins contain one (type I) or two (type II) conserved AAA+ domains, consisting of the ATPase domain with the Walker A (ATP binding) and Walker B (ATP hydrolysis) motifs followed by an α-helical C-domain (Ammelburg et al., 2006). AAA+ domains form a ring-shaped hexamer and thus there are 6 and 12 ATPase active sites in the type I and type II AAA+ proteins, respectively.

p97 (also known as VCP in mammals, CDC-48.1 and CDC-48.2 in *Caenorhabditis elegans*, and Cdc48p in yeast) is a highly conserved and abundant type II AAA+ protein. p97 plays essential roles in a number of cellular processes including membrane dynamics, cell cycle control, the ubiquitin-proteasome system, autophagy, and modulation of protein aggregates (for recent reviews, Stolz et al., 2011; Yamanaka et al., 2012; Meyer et al., 2012; Buchberger, 2013). Human p97 (VCP) has been linked to neurodegenerative disorders, hereditary inclusion body myopathy associated with Paget disease of bone and frontotemporal dementia (Watts et al., 2004; Weihl et al., 2009), and amyotrophic lateral sclerosis (Johnson et al., 2010). TAR DNA-binding protein 43-positive inclusions are accumulated in neuronal cells of the patients with both diseases (Johnson et al., 2010).

p97 consists of an N-terminal substrate/adaptor-binding domain followed by two AAA+ domains (D1 and D2) and forms a homo-hexameric double-ring structure. It has been shown that D2 mediates major ATPase activity (Song et al., 2003; DeLaBarre et al., 2006), and that the ATPase activity of D2 is critical for biological functions (Song et al., 2003; DeLaBarre et al., 2006; Esaki and Ogura, 2010; Nishikori et al., 2011). A quantitative analysis of nucleotide-binding to both D1 and D2 domains of rat p97 indicates that ATPγS, an ATP analog, binds to D1 and D2 with similar affinity, but ADP binds to D1 with higher affinity than to D2, which is consistent with the higher ATPase activity in D2 (Briggs et al., 2008). Stoichiometric measurements suggest that both ADP and ATPγS can saturate all six nucleotide binding sites in D1, but that only three to four of the six D2 sites can bind ATPγS simultaneously, and that ATPγS binding to the D2 domain triggers a downstream cooperative conformational change of at least three monomers (Briggs et al., 2008). The

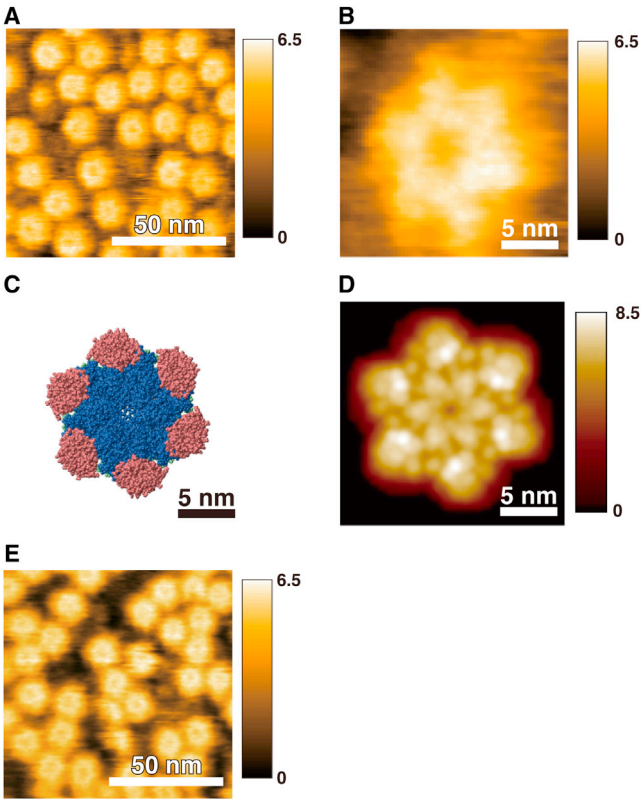

Figure 1. AFM Image of *C. elegans* CDC-48.1 Hexamers and Its Comparison with an Image of Mammalian p97 Simulated from the Crystal Structure

(A) A wide-area AFM image of CDC-48.1 hexamers without nucleotide. Scale bar, 50 nm.

(B) A filtered AFM image of a CDC-48.1 hexamer. Scale bar, 5 nm.

(C) The N-terminal side of the crystal structure of mouse apo p97 (PDB ID 3CF3; Davies et al., 2008). The N and D1 domains are magenta and blue, respectively. Scale bar, 5 nm.

(D) A simulated AFM image of the p97 hexamer constructed from the structure in C. Scale bar, 5 nm.

(E) A wide-area AFM image of ΔN CDC-48.1 hexamers without nucleotide. Scale bar, 50 nm. The brightness of all AFM images in this figure represents the sample height but is not linearly set to highlight the top surface structure. See also Figure S1.

D2 ATPase activity shows positive cooperativity (Nishikori et al., 2011). We recently found, using the yeast *Saccharomyces cerevisiae*, that cells with Cdc48p mutants deficient in ATP binding of D1 are able to grow, suggesting that ATPase deficiency of D1 does not affect the vital D2 ATPase activity in terms of essentiality (Esaki and Ogura, 2010). A systematic analysis of recombinant CDC-48.1 of *C. elegans* was performed to characterize the ATPase activity of D1 and D2 of CDC-48.1. Like mammalian p97, D2, but not D1, of CDC-48.1 showed strong ATPase activity with positive cooperativity at physiological temperature. The ATPase activity itself and its cooperativity of D2 are differently affected by ATPase-deficient mutations in D1. Interestingly, magnitude of the cooperativity of D2 is well related to growth rate of yeast cells. The D2 ATPase activity of p97 is operated in a nonstochastic fashion, and its positive cooperativity is critical for viability of the cell (Nishikori et al., 2011).

Crystal structures of p97 in different nucleotide states have been solved (DeLaBarre and Brunger, 2003; DeLaBarre et al., 2006; Huyton et al., 2003). Cryo-electron microscopy (EM) and small-angle X-ray scattering (SAXS) analyses also revealed conformations of p97 with different nucleotides (Zhang et al., 2000; Rouiller et al., 2000, 2002; Beuron et al., 2003; Davies et al., 2005). From these data, several models for conformational changes of p97 during the cycle of ATP hydrolysis have been proposed (for a review, see Pye et al., 2006). However, there have been no studies providing information about the dynamics of native p97 functioning in solution.

To depict conformational changes of p97 during the cycle of ATP hydrolysis in solution, we applied high-speed atomic force microscopy (AFM), a newly developed video-rate imaging technique, which enables to capture high-resolution images in millisecond time scales. By using high-speed AFM, several protein molecules such as myosin V, F_1-ATPase, and cellulase were analyzed and their linear or rotary movements were revealed in recent studies (Kodera et al., 2010; Uchihashi et al., 2011; Igarashi et al., 2011).

In this paper, we observed a *C. elegans* p97 CDC-48.1 immobilized on a mica surface with high-speed AFM. Clear images of CDC-48.1 ring-shaped hexamers with a narrow central pore were depicted and, in the presence of ATP, rotational movements of the D1 ring relative to the D2 ring were observed. The D1 ring repeatedly rotated ~23 ± 8° clockwise and returned to the original position. This rotational movement was strictly dependent on ATP, and ADP did not induce the rotation of wild-type CDC-48.1. Mutational analysis revealed that the ring rotation was induced by ATP-binding to the D2 domain. The molecular mechanism of p97, in which ATP-binding to the D2 domain induces conformational change, that in turn gives a twist at the linker between the N-D1 and D2 domains, has been suggested. Taken together, our demonstration of functioning p97 with high-speed AFM provides insight into the molecular mechanism of p97.

RESULTS

High-Speed AFM Observation of a *C. elegans* p97 ATPase, CDC-48.1

Purified N-terminally His-tagged wild-type CDC-48.1, a *C. elegans* p97 ATPase, was directly immobilized on a surface of mica (Figure S1A available online), and was observed with high-speed AFM. Images of observed p97 particles were apparently homogeneous hexameric rings of ~18.3 ± 1.7 nm in diameter (Figures 1A and 1B). The observed image of the CDC-48.1 hexamer (Figure 1B) looks similar to an image of the N-D1 side of mouse p97 (Figure 1D), which was simulated from the crystal structure (Figure 1C; Davies et al., 2008), and its size is roughly consistent with that of the simulated image. To confirm the notion that the N-D1 side is observed under the conditions used here, a mutant CDC-48.1 lacking the N domain was also purified and observed with high-speed AFM. We found that images showed homogeneous hexameric rings of ~15.3 ± 1.6 nm in diameter (Figure 1E), which is significantly smaller than that of the full-length wild-type. Considering these lines of evidence together, we conclude that the C-terminal part of CDC-48.1 was, at least predominantly, immobilized, and

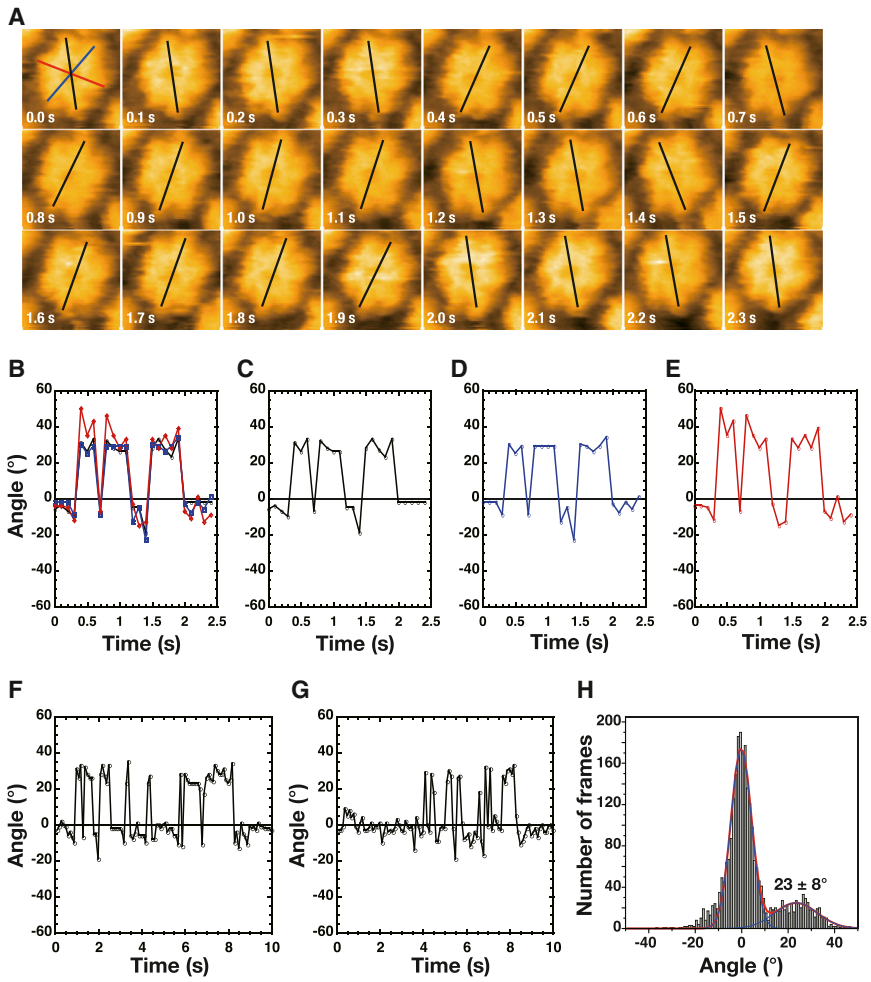

Figure 2. ATP-Dependent Rotational Movements of Wild-Type CDC-48.1 Hexamers

(A) Successive AFM images of a wild-type CDC-48.1 hexamer taken in the presence of 3 mM ATP (Movie S1). Three diametric lines colored differently are indicated in the first image (0.0 s). Only one of these lines (black) is indicated in other images for simplicity.

See also Figure S2A.

(B–E) Time course of angular variation of diametric lines in the successive images shown in (A) is shown. Clockwise rotation is indicated by plus degrees, and counterclockwise one is indicated by minus degrees. Graphs of three lines are overlaid in (B), and each is separately shown in (C), (D), and (E).

(F and G) Two representative 10 s time courses show repeated rotational movements. The first 2.5 s graph of (F) corresponds to that of (C; note the difference in time scale). Longer time courses containing these two examples and additional time courses are shown in Figures S2B–S2E.

(H) Histogram of the angle of diametric lines of wild-type CDC-48.1 hexamers in the presence of 3 mM ATP. Number of hexamers observed = 9; total observation period = 107.8 s. Red line, double-Gaussian fit result; blue lines, Gaussian components in double-Gaussian fit. Peak value represents mean ± SD analyzed and calculated using Origin 6.0 software.

See also Figures S2F–S2I and Movie S2 for movements of wild-type CDC48.1 hexamers lacking one protomer.

therefore that the N-D1 side was depicted when CDC-48.1 was immobilized directly. To further confirm this notion, we tried to immobilize CDC-48.1 by using its N-terminal His-tag. The N-terminally His-tagged CDC-48.1 was immobilized on a surface of streptavidin crystals through binding of His-tag to Ni-NTA-biotin attached to streptavidin (Figure S1C). Images showed rings of ~15.0 ± 1.4 nm in diameter, which is smaller than that of the directly immobilized full-length wild-type, and fits with the size of the D2 ring reasonably well.

As shown in Figure 1, the images of the N-D1 side of CDC-48.1 hexamers immobilized directly on a surface of mica clearly indicate a 6-fold symmetric ring with a narrow central pore. The height of CDC-48.1 hexamers was ~5.7 ± 0.7 nm, which was significantly shorter than those (8.4–11.0 nm) of the crystal structures of mammalian p97. Therefore, human p97 was purified and observed. The height of the human p97 ring was ~6.4 ± 0.7 nm, which was significantly taller than that of the CDC-48.1 ring, but still shorter than those of the crystal structures of rat p97. The reason for the difference in height between AFM images and crystal structures is uncertain. On the other hand, the images of the D2 side of CDC-48.1 hexamers were enough for measurement of diameter as described above, but unfortunately not sufficient for precise analysis of shape, perhaps due to lateral diffusion of the lipid bilayer. Therefore, we decided to analyze conformational changes of the N-D1 side of CDC-48.1 hexamers in detail.

ATP Induces Rotation of the N-D1 Ring of CDC-48.1

To achieve high-resolution video-rate observation of CDC-48.1 hexamers, the images of CDC-48.1 were taken with a frame capture time of 100 ms unless otherwise specified. In the presence of 3 mM ATP, rotational movements, which were distinguishable from irregular Brownian motions, were repeatedly observed (Figure 2; Movie S1) for roughly 30%–40% of hexameric rings of CDC-48.1. In a series of typical images (Figure 2A), changes in the angle of three diametric lines that go through the centers of opposite D1 subunits were measured (Figures 2B–2E). The N-D1 ring rotated ~23 ± 8° clockwise relative to the D2 ring immobilized to a mica surface, stayed in the rotated position for 0.1 s or more, and returned to the original position (Figures 2F and 2G). In the rotated state, all three diametric lines are similarly at the rotated position (Figures 2C–2E), indicating that the 6-fold symmetry of the N-D1 ring is essentially unchanged during the course of movements. Reliability of the above analysis has been verified by the image analysis using EMAN1's boxer and SPIDER programs, both of which are frequently applied for analysis of electron microscopic images (Figure S2A).

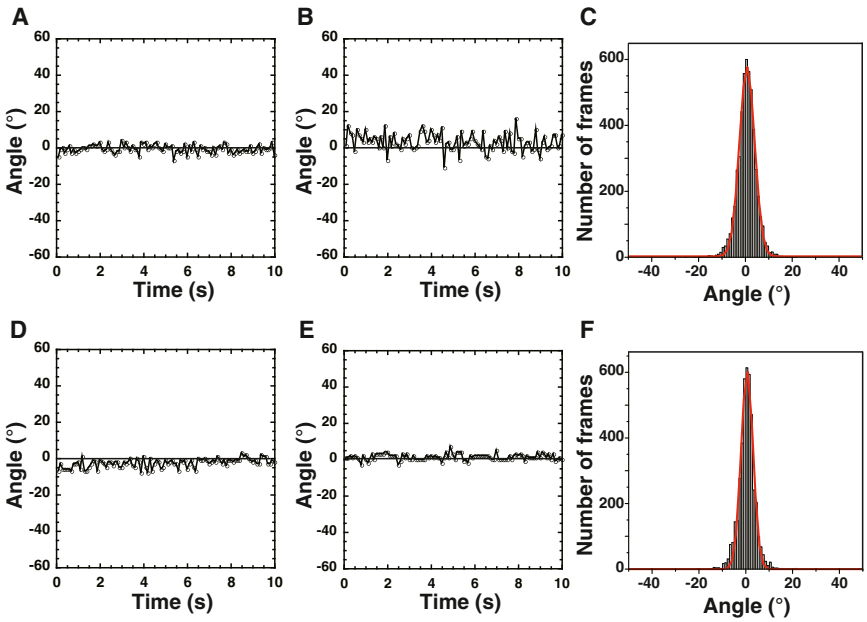

Figure 3. Movements of Wild-Type CDC-48.1 Hexamers in the Absence of Nucleotide and in the Presence of 3 mM ADP

AFM images are taken and analyzed as in Figure 2.

(A and B) Two representative 10 s time courses of wild-type CDC-48.1 hexamers in the absence of nucleotide are shown (Movie S3).

(C) Histogram of the angle of diametric lines of wild-type CDC-48.1 hexamers in the absence of nucleotide. Number of hexamers observed = 10; total observation period = 164.8 s. Red line, single-Gaussian fit result. Longer time courses containing these two examples and additional other time courses are shown in Figures S3A–S3D.

(D and E) Two representative 10 s time courses of wild-type CDC-48.1 hexamers in the presence of 3 mM ADP are shown (Movie S4).

(F) Histogram of the angle of diametric lines of wild-type CDC-48.1 hexamers in the presence of ADP. Number of hexamers observed = 10; total observation period = 139.5 s. Red line, single-Gaussian fit result. Longer time courses containing these two examples and additional time courses are shown in Figures S3E–S3H.

Distributions of the line angle measured for nine independent hexamers, which showed significant rotational movements during the observation (total observation period was 107.8 s; Figures S2B–S2E for four out of nine), are shown in Figure 2H. There are two peaks at positions 0° (resting state) and 23° (rotated position). From the distributions, the rotational movement seems to be a single 23° step with no evidence of substeps. Since the periodicity in a hexamer is 60°, a 23° clockwise rotation appears equivalent to a 37° counterclockwise rotation. To discriminate between these possibilities, it is necessary to label a hexamer asymmetrically. During the observation with high-speed AFM, we noticed that some hexamers accidentally lost one subunit and continued to move for a couple of seconds, and that they finally disassembled and disappeared from the visual field (Figures S2F–S2I; Movie S2). From these results, we conclude that the rotation is 23 ± 8° in the clockwise direction.

Under the present conditions, we are unable to observe the conformational changes of the D2 domain. As described later, the observed rotational movement depends on ATP-binding to the D2 domain. Therefore, it is most likely that ATP binding to the D2 domain induces its conformational changes, leading to the clockwise rotation of the D2 ring relative to the N-D1 ring when observed from the bottom. This movement results in the clockwise rotation of the N-D1 ring relative to the D2 ring immobilized on a surface of mica when observed from the top.

Rotation of the N-D1 Ring Depends on ATP

To know the nucleotide dependency of the rotational movement of the N-D1 ring, we observed CDC-48.1 in the absence of nucleotide and the presence of 3 mM ADP. Because the symmetry of the hexamers was again unchanged, changes in the angle of only one diametric line were shown for simplicity. In both cases, large rotational movements, as in the case of the presence of ATP, were not observed (see Figures 3A–3C for no nucleotide and Figures 3D–3F for ADP; Figure S3; Movies S3 and S4). Therefore, we conclude that the ~23 ± 8° clockwise rotation of the N-D1 ring strictly depends on the presence of ATP.

Lower ATP Concentration Decreases Abundance of Rotated State

AFM experiments were performed in the presence of a lower concentration of ATP, 0.3 mM (Figure 4). The clockwise rotations were again observed (Figures 4A and 4B; Figure S4), and the peak of the rotated position was ~19 ± 10° (Figure 4C). The peak of the rotated position (the number of frames in the rotated state) was significantly lower than that in the presence of 3 mM ATP (Figure 2H). To compare the kinetics at different concentrations of ATP precisely, we measured dwell time in the resting state and lifetime of the rotated state (Figures S4E–S4H). These time distributions are fitted to sums of two exponential decay functions. While dwell time in the resting state, which corresponds to the time waiting for ATP binding, in the presence of 0.3 mM ATP was slightly longer than that in the presence of 3 mM ATP (Figures S4E and S4F), lifetime of the rotated state, which corresponds to the time ATP remains bound, was significantly shortened by the decrease of the ATP concentration as evident by an ~80% decrease of preexponential factor A_2 of time constant τ_2 (Figures S4G and S4H).

Rotation of N-D1 Depends on Binding of ATP to the D2 Domain

Which domain is responsible for the rotational movement? Does ATP binding induce it, or is ATP hydrolysis required? To address these important questions, we analyzed two mutant CDC-48.1 proteins, CDC-48.1^{K530A} and CDC-48.1^{E584Q}, with high-speed AFM. It has been indicated that the D2 domain of p97 shows major ATPase activity and the D1 domain, which is responsible for stable hexamerization, shows only weak ATPase activity (Song et al., 2003; DeLaBarre et al., 2006). Crystal structural analysis has indicated that purified p97 hexamers contain six ADP bound to the D1 domain (DeLaBarre and

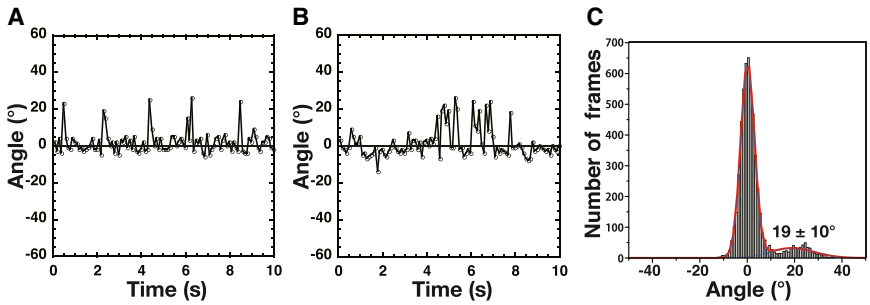

Figure 4. Movements of Wild-Type CDC-48.1 Hexamers in the Presence of 0.3 mM ATP

AFM images are taken and analyzed as in Figure 2.

(A and B) Two representative 10 s time courses of wild-type CDC-48.1 hexamers in the presence of 0.3 mM ATP are shown.

(C) Histogram of the angle of diametric lines of wild-type CDC-48.1 hexamers in the presence of 0.3 mM ATP. Number of hexamers observed = 10; total observation period = 179.8 s. Red line, double-Gaussian fit result; blue lines, Gaussian components in double-Gaussian fit. Peak value represents mean ± SD. Longer time courses containing these two examples and additional time courses are shown in Figures S4A–S4D.

See also Figures S4E–S4H for histograms of dwell time in the resting state and lifetime of the rotated state.

Brunger, 2003; Huyton et al., 2003). It has also been shown that ATP binding to the D2 domain induces conformational changes of p97 (Zhang et al., 2000; Rouiller et al., 2000). Therefore, it is reasonable to assume that the rotational movement is induced by the ATP binding to the D2 domain. CDC-48.1^{K530A} and CDC-48.1^{E584Q} are Walker A and Walker B mutants of the D2 domain, which are defective in ATP-binding and ATP-hydrolysis, respectively.

As expected, Walker A mutant CDC-48.1^{K530A} did not show the rotational movement in the presence of ATP (Figures 5A–5C for ATP, and Figures 5D–5F for ADP; Figure S5), indicating that the ATP binding to the D2 domain is essential for the rotational movement. To know whether ATP hydrolysis is required for the rotational movement, we then observed Walker B mutant CDC-48.1^{E584Q} in the presence of 3 mM ATP by high-speed AFM. Images showed repeated rotational movements of the N-D1 ring of CDC-48.1^{E584Q} (Figures 6A–6C; Figures S6A–S6D), indicating clearly that ATP binding, but not hydrolysis, is necessary to induce the rotational movement. We then also observed this mutant in the presence of 3 mM ADP. Surprisingly, the N-D1 domain of CDC-48.1^{E584Q} rotated clockwise repeatedly (Figures 6D–6F; Figures S6E–S6H). The observed rotation angles of the mutant CDC-48.1^{E584Q} in the presence of ATP and ADP were ~20 ± 6° (Figure 6C) and ~22 ± 4° (Figure 6F), respectively, and was similar to that of wild-type CDC-48.1 in the presence of ATP (~23 ± 8°).

DISCUSSION

We have successfully observed and captured video-rate images of nucleotide-induced conformational changes of a multifunctional molecular chaperone CDC-48.1, a *C. elegans* p97 homolog, in solution by high-speed AFM. The observed conformational changes were mainly forward clockwise and backward counterclockwise rotational movements between the N-D1 and D2 hexameric rings. Mutational analysis indicates that ATP-binding to the D2 domain induces the clockwise ~23 ± 8° rotation of the N-D1 ring relative to the D2 ring; in other words, the counterclockwise rotation of the D2 ring relative to the N-D1 domain when observed from N-D1. Because ATP binding to the D2 domain is responsible for this rotation, it is reasonable to assume that the observed conformational changes are induced by changes in the D2 domain. Unfortunately, however, in the present study conformational changes in the D2 ring were not seen, because the D2 domain was immobilized onto a surface of mica. Rotational movements between the N-D1 and D2 rings of p97 have been suggested by cryo-EM and SAXS studies (Zhang et al., 2000; Davies et al., 2005). Our high-speed AFM data are essentially consistent with SAXS data by Davies et al. (2005). It should be emphasized that our study reveals ATP-dependent dynamic conformational changes of active p97 in an aqueous solution in real time.

It has been suggested that p97 promotes segregation of substrate proteins and disassembly of protein complexes. Repeated back and forward rotational movements of p97 may account for, at least in part, mechanical force in such processes. In contrast to AAA+ regulatory subunits of ATP-dependent proteases such as ClpA and ClpX, which are often referred to as unfoldases, there has been no convincing evidence for a threading mechanism, in which substrates are completely unfolded by threading through the central pore, for p97, although it has recently been suggested that archaeal Cdc48 homologs thread substrates as discussed below. Instead, at least, two distinct mechanisms have been proposed for p97; a "D2 in – D2 out" model, in which substrates enter and exit the pore at the D2 domain, and a "surface only" model, in which the pronounced domain movements of p97 during the cycle of ATP hydrolysis segregate or extract substrates (Buchberger, 2013). Our present study clearly demonstrates that p97 undergoes obvious domain movements, and supports the surface-only model for the p97 activity. Importantly, however, our present data do not exclude any other models. In fact, recent studies suggest that archaeal Cdc48 homologs can thread substrates (Barthelme and Sauer, 2012, 2013; Forouzan et al., 2012).

From crystal structural and cryo-EM studies, it has also been suggested that the N domain of p97 is highly mobile (Rouiller et al., 2002; DeLaBarre and Brunger, 2003). We have carefully analyzed changes in the shape and height of the N-D1 ring during the rotational movements in the presence of ATP, but we have failed to detect any significant differences in them, indicating that motions of the N domain are minimum or so rapid and below the limit of detection, if any.

There are six identical ATPase domains in the D2 hexameric ring. Briggs and colleagues have demonstrated that only three to four of the six D2 sites can bind ATPγS simultaneously, and that ATPγS binding triggers a cooperative conformational change of at least three D2 monomers (Briggs et al., 2008). They also found that ATPγS binding to D2 is consistent with a

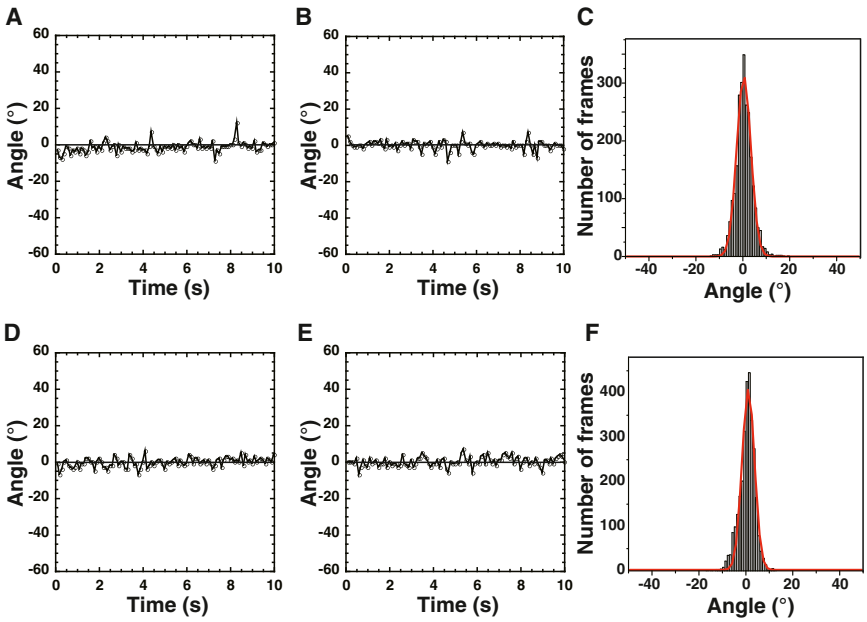

Figure 5. Movements of Walker A Mutant CDC-48.1^{K530A} Hexamers in the Presence of 3 mM ATP or ADP

AFM images are taken and analyzed as in Figure 2.

(A and B) Two representative 10 s time courses of CDC-48.1^{K530A} hexamers in the presence of 3 mM ATP are shown.

(C) Histogram of the angle of diametric lines of CDC-48.1^{K530A} hexamers in the presence of 3 mM ATP. Number of hexamers observed = 10; total observation period = 82.6 s. Red line, single-Gaussian fit result. Longer time courses containing these two examples and additional time courses are shown in Figures S5A–S5D.

(D and E) Two representative 10 s time courses of CDC-48.1^{K530A} hexamers in the presence of 3 mM ADP are shown.

(F) Histogram of the angle of diametric lines of CDC-48.1^{K530A} hexamers in the presence of 3 mM ADP. Number of hexamers observed = 10; total observation period = 97.9 s. Red line, single-Gaussian fit result. Longer time courses containing these two examples and additional time courses are shown in Figures S5E–S5H.

two-site model with high- and low-affinity sites. For simplicity, we assume here that four ATP molecules bind to the D2 ring maximally and that two ATP molecules bind to D2 with a high affinity, then an additional two ATP molecules bind with a low affinity (Figure 7 for models). Our video imaging of CDC-48.1 in the presence of ATP shows that the rotation of the N-D1 ring relative to the D2 ring is a single step event, indicating that this rotation seems to occur suddenly and to a fixed extent (~23 ± 8°) upon binding of ATP to the D2 domain. We also predict that the binding of the third ATP induces the ~23 ± 8° clockwise rotation of the D2 ring, and that the D2 ring with the bound three to four ATP molecules stays in the rotated position. This prediction is consistent with conformational changes determined by SAXS analysis by Davies and colleagues (Davies et al., 2005). They observed the ~20° clockwise rotation of the D2 ring upon saturation by AMP-PNP.

ATP hydrolysis may occur in a coordinated manner or stochastically. We have recently reported that the ATPase activity of D2 is cooperative, and that this cooperativity is critical for essential functions of p97 (Nishikori et al., 2011). Model WT (Figure 7) implies that two or four ATP molecules are hydrolyzed simultaneously, and it suggests a cooperative mode of ATP hydrolysis. This model also suggests that the D2 ring returns to the original position (resting state) upon the hydrolysis of ATP, since the number of ATP molecules decreases to two or zero.

The histogram of lifetime of wild-type in the rotated state in the presence of 3 mM ATP fits to a sum of two exponential curves with preexponential factors of A_1 = 353 s^{-1} and A_2 = 59 s^{-1} and time constants of τ_1 = 0.066 s and τ_2 = 0.32 s (Figure S4G; Table S1). Two exponential distributions were statistically significant judging from the *F*-test result ($p < 0.01$). According to Model WT, rate constants can be determined as described in the Experimental Procedures.

Rate constants obtained for wild-type in the presence of 3 mM ATP were k_{-2} = 10.0 s^{-1}, k_3 = 4.7 s^{-1}, and k_{-3} = 2.1 s^{-1} (Figure 7). Preexponential factors and time constants calculated using these values in the presence of 3 mM or 0.3 mM ATP were consistent with the experimentally determined values (Table S1). Therefore, Model WT accounts for changes in the distribution of lifetime of the rotated state.

Do the observed repeated clockwise and counterclockwise rotational movements represent the movements during cycles of ATP hydrolysis? Because a Walker B motif mutant CDC-48.1^{E584Q}, which is defective in ATP hydrolysis in the D2 domain, also shows frequent rotational movements as similar as wild-type CDC-48.1 (Figure 6), it is evident that ATP binding and dissociation significantly contribute to repeated rotational movements of wild-type hexamers. In Model WT, hexamers in state 2 are converted to those in the resting state either by dissociating one ATP molecule indicated as state 1 or by hydrolyzing ATP molecules indicated as state 4. Using the rate constants k_{-2}, k_{-3}, k_3, and k_4 of wild-type in the presence of 3 mM ATP, ratio of hexamers that underwent ATP hydrolysis in the D2 domain was calculated to be ~19%, suggesting that the majority of observed movements of wild-type hexamers are induced by ATP binding and dissociation under the conditions used. Immobilization of CDC-48.1 to a surface of mica may affect its ATPase activity. Indeed, it was found that CDC-48.1 immobilized to mica showed a reduced ATPase activity, approximately one fifth of that measured in solution (data not shown). Frequent dissociation of the bound ATP molecules simply induces repeated rotational movements of hexamers even in the case of CDC-48.1^{E584Q}. Under physiological conditions, CDC-48.1^{E584Q} would remain rotated longer, because it is unable to hydrolyze ATP and dissociation of ATP would be much slower. Wild-type CDC-48.1 can hydrolyze ATP, and therefore it would return to the resting state predominantly by hydrolysis of ATP. The cycle of ATP hydrolysis ensures frequent repeated back and forth rotational movements, which may produce mechanical force to disassembly of substrate protein complexes.

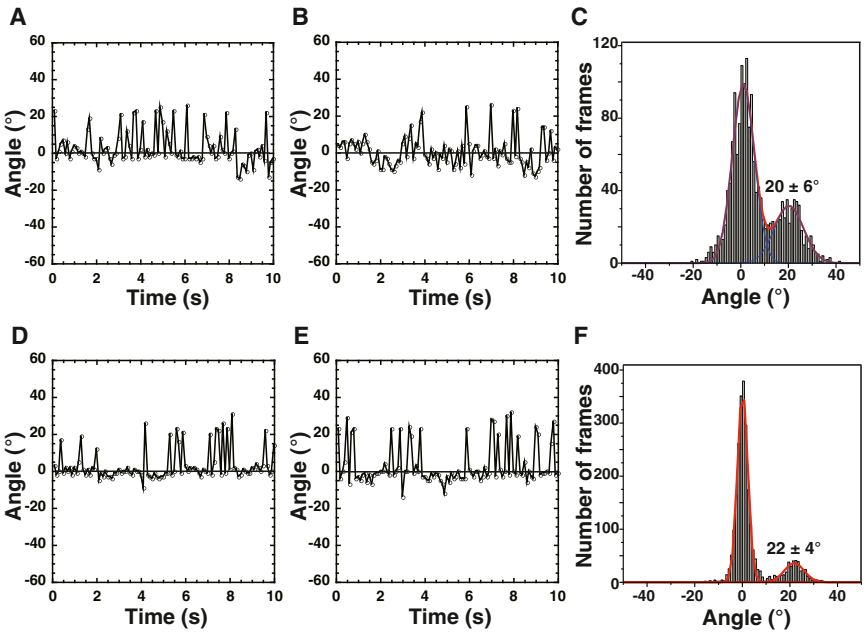

Figure 6. Walker B Mutant CDC-48.1^{E584Q} Hexamers Rotate in the Presence of 3 mM ATP or even ADP

AFM images are taken and analyzed as in Figure 2.

(A and B) Two representative 10 s time courses of CDC-48.1^{E584Q} hexamers in the presence of 3 mM ATP.

(C) Histogram of the angle of diametric lines of CDC-48.1^{E584Q} hexamers in the presence of 3 mM ATP. Number of hexamers observed = 10; total observation period = 55.5 s. Red line, double-Gaussian fit result; blue lines, Gaussian components in double-Gaussian fit. Peak value represents mean ± SD. Longer time courses containing these two examples and additional time courses are shown in Figures S6A–S6D.

(D and E) Two representative 10 s time courses of CDC-48.1^{E584Q} hexamers in the presence of 3 mM ADP.

(F) Histogram of the angle of diametric lines of CDC-48.1^{E584Q} hexamers in the presence of 3 mM ADP. Number of hexamers observed = 10; total observation period = 83.5 s. Red line, double-Gaussian fit result; blue lines, Gaussian components in double-Gaussian fit. Peak value represents mean ± SD. Longer time courses containing these two examples and additional time courses are shown in Figures S6E–S6H.

See also Figures S6I and S6J for histograms of dwell time in the resting state and lifetime of the rotated state, respectively.

In this respect, recent findings on *N*-ethylmaleimide-sensitive factor (NSF), another type II AAA+ chaperone, which disassembles the soluble NSF attachment protein (SNAP) receptor (SNARE) complex in an ATP-dependent manner, are highly intriguing. Using single-particle cryo-EM and negative-stain EM, Chang and colleagues (Chang et al., 2012) found that ATP hydrolysis induces an ~22° counterclockwise rotation of the D1 ring relative to the D2 ring, and they suggest that this rotation is related to a possible mechanism for converting chemical energy from ATP hydrolysis into mechanical work in the SNARE complex disassembly (Chang et al., 2012). Because the D1 ring of p97 rotates ~23 ± 8° clockwise upon ATP-binding and returns to the original position (a ~23 ± 8° counterclockwise rotation) upon ATP hydrolysis as described above, both the direction and extent of the rotation in NSF upon ATP hydrolysis are fully consistent with those in p97, suggesting that the molecular mechanisms underlying disassembly of protein complexes by NSF and p97 may be fundamentally similar. It should be noted, however, that the catalytically active ATPase domains are different in NSF and p97. D1 is active and D2 is inactive in ATP hydrolysis in NSF, while D2 is efficient and D1 is inefficient in p97.

Rate constants obtained for CDC-48.1^{E584Q} in the presence of 3 mM ATP were k_{-2} = 8.2 s^{-1}, k_3 = 0.43 s^{-1}, and k_{-3} = 0.72 s^{-1} (Figure 7; Table S1; Model E584Q). Rate constants k_3 (0.43 s^{-1}) and k_{-3} (0.72 s^{-1}) are roughly one tenth and one third of the wild-type values (4.7 s^{-1} and 2.1 s^{-1}, respectively), whereas rate constant k_{-2} (8.2 s^{-1}) is similar to the wild-type value (10.0 s^{-1}). A simple explanation for CDC-48.1^{E584Q} is that the binding affinity of the fourth ATP to the mutant is much lower than that of wild-type. Glu584 is the catalytic glutamate in D2 and therefore senses the γ phosphate of the bound ATP. This signaling may facilitate the binding of the fourth ATP. In mutant CDC-48.1^{E584Q}, the signaling is defective and the binding of the fourth ATP may therefore be slow. The γ phosphate sensing by the Glu584 residue may be a key regulatory mechanism of the rotational movement. For AAA+ proteins, the glutamate switch has been proposed (Zhang and Wigley, 2008). The glutamate switch regulates ATPase activity in response to the binding of target ligands by controlling the orientation of the catalytic Glu residue, switching it between active and inactive conformations. In the case of p97, the D2 domain, which is not directly involved in substrate binding, interacts with the D1 domain through a region, where the glutamate switch exists, in the D2 domain. The glutamate switch has also been identified in T7 DNA helicase, which is distinct from but related to AAA+ proteins (Satapathy and Richardson, 2011). It has been revealed that the glutamate switch of T7 DNA helicase couples dTTP hydrolysis to DNA binding, and that, when the catalytic Glu residue is replaced with glutamine, which is unable to sense the γ phosphate, the altered helicase, unlike the wild-type helicase, binds DNA in the presence of dTDP. Therefore, it is reasonably assumed that the rotation of CDC-48.1^{E584Q} may be induced by ADP as well as ATP by a similar mechanism. Further studies are needed to elucidate the detail of this regulatory mechanism.

Recently, conformational changes of F_1 ATPase have been extensively investigated by high-speed AFM (Uchihashi et al., 2011). F_1 ATPase is also a Walker-type hexameric ATPase of the RecA fold as well as AAA+ family ATPases (Lupas and Martin, 2002). F_1 is a motor in which three torque-generating β subunits in the $\alpha_3\beta_3$ stator ring sequentially undergo conformational changes upon ATP hydrolysis to rotate the central shaft γ

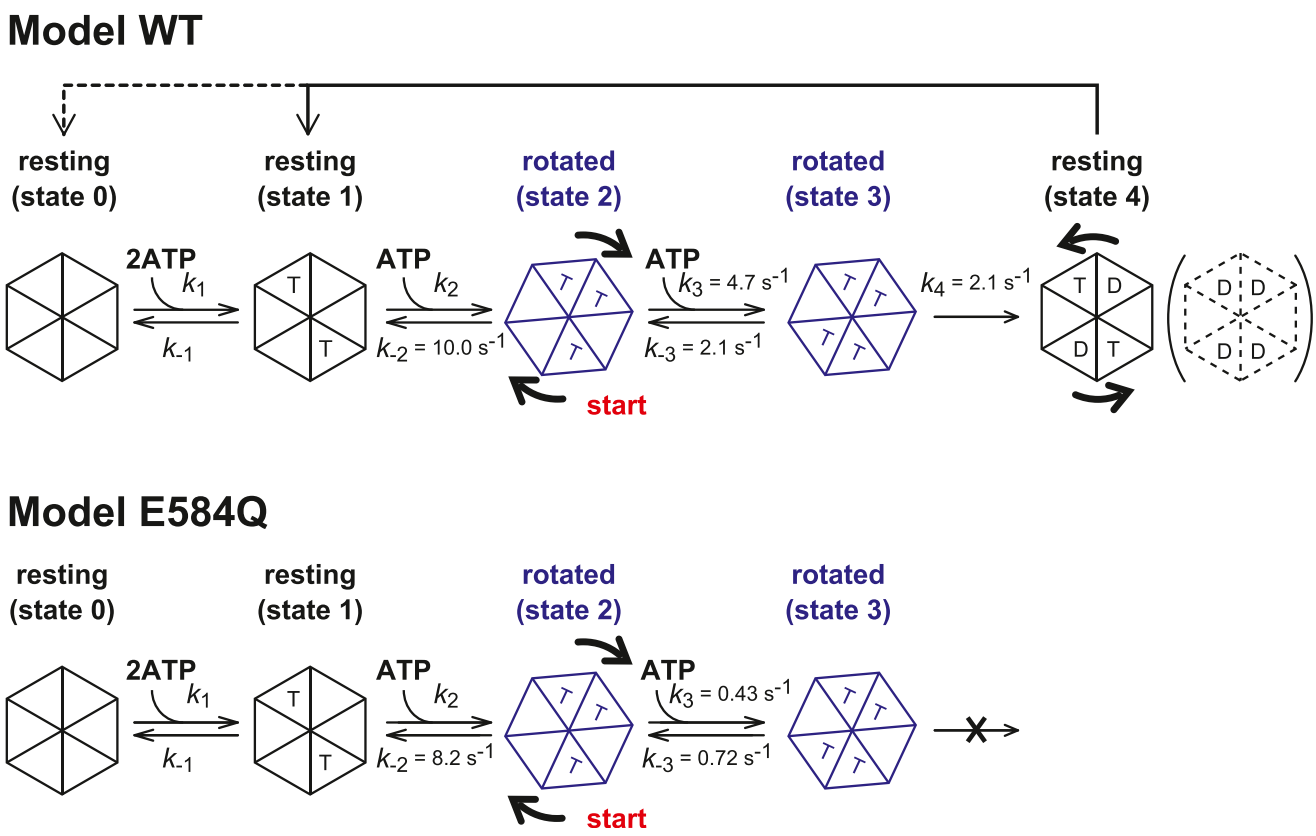

Figure 7. Models for Nucleotide-Induced Rotation of CDC-48.1

Bottom views of CDC-48.1 hexamers and their predicted nucleotide states are schematically depicted. Models imply that ATP-binding to D2 induces conformational changes of the D2 domain, and the conformational changes of D2 result in twisting motion between the D2 and N-D1 rings. The D2 ring rotates ~23 ± 8° clockwise relative to the N-D1 ring when observed from the bottom. In the present high-speed AFM observation, however, the D2 ring is fixed on a surface of mica, and therefore the D2 cannot be observed. Instead, the N-D1 side is observed, and the N-D1 ring rotates ~23 ± 8° clockwise when observed from the top. The N-D1 ring and conformational changes in the D2 domain, except for the rotational movements of the D2 ring, are not drawn for simplicity. There are two states, resting and rotated states. T represents ATP, and D represents ADP. The rotated state starts at state 2, where the third ATP binds to the D2 ring. Rate constants, which are related to the lifetime of rotated state, were determined from the data of histogram of the lifetime of wild-type CDC-48.1 in the rotated position in the presence of 3 mM ATP (Figure S4G) for Model WT, and from that of CDC-48.1^{E584Q} in the rotated position in the presence of 3 mM ATP (Figure S6J) for Model E584Q. See also Table S1.

unidirectionally. It has been shown that the rotorless F_1 still "rotates," i.e., the three β subunits in the isolated $\alpha_3\beta_3$ stator ring cyclically propagate conformational states in the counterclockwise direction, similar to the rotary shaft rotation in F_1 (Uchihashi et al., 2011). Obviously, β subunits of F_1 themselves undergo significant conformational changes during the cycle of ATP hydrolysis. Unfortunately, however, it is uncertain whether CDC-48.1 subunits undergo conformational changes during the cycle of ATP hydrolysis, because the D2 ring of CDC-48.1 is fixed to the surface of mica under the conditions used, and it is impossible to observe the D2 ring. Immobilization of the N-terminal side of CDC-48.1 to mica allows observation of the D2 ring. Indeed, the N-terminally His-tagged CDC-48.1 could be immobilized through binding of His-tag to Ni-NTA-biotin as described, but the resolution of captured images of the D2 ring has been low. It is clear that the rotation of F_1 ring is sequential and unidirectional under certain conditions, but the rotation of CDC-48.1 is a single-step back and forth in a twisting motion between covalently connected two rings. Both F_1 and CDC-48.1 are hexameric and structurally related, but modes of conformational changes seem to be significantly different. Each subunit of F_1 has a single ATPase domain, whereas CDC-48.1 has two ATPase domains in tandem.

Here, we establish the methodology to visualize structure and movement of hexameric chaperones functioning in solution simultaneously with high-speed AFM, which reveals nucleotide-induced conformational changes in a millisecond time scale. Our results provide insights into the molecular mechanism of the molecular chaperone, p97. In a future study, we would like to improve procedures of immobilization of the N domain of CDC-48.1 to a surface of mica to visualize the shape of the D2 ring more clearly with high-speed AFM, which may allow us to observe conformational changes of the D2 ring with a high ATPase activity precisely.

EXPERIMENTAL PROCEDURES

Preparation of *C. elegans* CDC-48.1 Variants and Human VCP

Plasmids expressing His-tagged CDC-48.1 mutants and His-tagged human VCP were constructed using the QuikChange kit (Stratagene). N-terminally

His-tagged wild-type and mutant CDC-48.1 proteins, and N-terminally His-tagged human VCP were expressed in insect cells and purified as described previously (Nishikori et al., 2011).

ATPase Assay

ATPase activity was determined using the malachite green assay (Chan et al., 1986) as described previously (Nishikori et al., 2011).

Fixation of CDC-48.1 and VCP onto Mica for AFM Observation

A droplet containing CDC-48.1 or VCP (~10 nM) was deposited on a surface of untreated mica for 10 min, followed by washing with buffer A (50 mM Tris-HCl [pH 8.0], 50 mM KCl, 30 mM β-mercaptoethanol, and 5 mM $MgCl_2$). To prepare a Ni-NTA coated mica, streptavidin two-dimensional (2D) crystals were formed on supported biotin-containing lipid bilayer as described previously (Yamamoto et al., 2009), and Ni-NTA-biotin was attached to streptavidin by depositing a droplet containing 0.1 mM Ni-NTA-biotin for 5 min. The sample stage was mounted on the AFM head and immersed in buffer A with or without ATP or ADP.

High-Speed AFM Apparatus

We used a home-built high-speed AFM apparatus (Ando et al., 2001; 2008). The cantilevers (Olympus) were 6–7 μm long, 2 μm wide, and 90 nm thick. Their spring constant was ~0.1 Nm^{-1}, and their resonant frequency and quality factor in water were 0.8–1 MHz and ~2, respectively. For AFM imaging, the free oscillation amplitude was ~1 nm and the set-point amplitude was around 90% of the free oscillation amplitude. The tapping force estimated was less than 30 pN (Rodriguez and Garcia, 2003). The probe tip was grown on the tip of a cantilever with electron beam deposition and was further sharpened by argon plasma etching (Wendel et al., 1995).

AFM Imaging and Image Processing

All AFM observations were performed at room temperature (24°C–26°C). We usually used a scan area of 40 × 20 or 40 × 40 nm^2 with 128 × 64 or 128 × 128 pixels. The AFM images were captured at frame rates of 10 fps. A 3 × 3 pixel-average filter was applied to each tracked image to reduce noise.

Simulation of AFM Image

We used software (SPM simulator, Advanced Algorithm Systems, Tokyo, Japan) to simulate AFM images of the p97 hexamer attached to a surface of mica. The simulation was carried out with a simple hard-sphere model as described (Uchihashi et al., 2011). The cantilever tip was modeled as a circular cone (apex angle, 30°) with a small sphere (radius, 8 nm) at the apex. Crystal structure of the apo p97 (Protein Data Bank [PDB] ID: 3CF3; Davies et al., 2008) was used as the sample. Each atom in the protein was modeled as a hard sphere with a corresponding van der Waals radius. We simulated AFM images using various radii for the tip-apex sphere and found that a radius of 8 nm produced the images most similar to the actual AFM images. The simulated images were processed by a low-pass filter with a cut-off wavelength of 2 nm, because the spatial resolution of the AFM image was approximately 2 nm judging from the 2D Fourier transformation of actual AFM images.

Determination of Kinetic Parameters

Kinetic parameters were determined by fitting double exponentials to histograms using the software Origin 6.0 (Lightstone, Tokyo, Japan) as follows. The histograms of the dwell time in the resting state and the lifetime of rotated state of wild-type CDC-48.1 (Figure S4) and CDC-48.1^{E584Q} (Figure S6) were fitted by the following equation to determine the preexponential factors and time constants in each exponential term (see also the left column of Table S1)

$$n(t) = A_1 \exp\left(-\frac{t}{\tau_1}\right) + A_2 \exp\left(-\frac{t}{\tau_2}\right), \qquad \text{(Equation 1)}$$

where $n(t)$ is the number of event that occurred during time interval between t and $t + dt$.

To determine the rate constants indicated in Model WT in Figure 7, the histograms of the lifetime of rotated state of wild-type CDC-48.1 in the presence of 3mM ATP (Figure S4G) were fitted by

$$n(t) = C\left\{k_{-2} + \left(k_{-2} + k_3 - \frac{1}{\tau_1}\right)\frac{k_4}{k_{-3}}\right\}\frac{k_{-2} + k_3 - 1/\tau_2}{1/\tau_1 - 1/\tau_2}\exp\left(-\frac{t}{\tau_1}\right) + C\left\{k_{-2} + \left(k_{-2} + k_3 - \frac{1}{\tau_2}\right)\frac{k_4}{k_{-3}}\right\}\frac{k_{-2} + k_3 - 1/\tau_1}{1/\tau_2 - 1/\tau_1}\exp\left(-\frac{t}{\tau_2}\right), \qquad \text{(Equation 2)}$$

where C is constant, and time constants τ_1 and τ_2 are given by

$$\tau_1 = \left\{\frac{1}{2}\left(k_{-2} + k_3 + k_{-3} + k_4 + \sqrt{(k_{-2} + k_3 - k_{-3} - k_4)^2 + 4k_3k_{-3}}\right)\right\}^{-1} \qquad \text{(Equation 3)}$$

and

$$\tau_2 = \left\{\frac{1}{2}\left(k_{-2} + k_3 + k_{-3} + k_4 - \sqrt{(k_{-2} + k_3 - k_{-3} - k_4)^2 + 4k_3k_{-3}}\right)\right\}^{-1}. \qquad \text{(Equation 4)}$$

For Model E584Q, the rate constants are determined by fitting the following equation to the histogram of the lifetime of rotated state of CDC-48.1^{E584Q} in the presence of 3mM ATP (Figure S6J)

$$n(t) = C\,k_{-2}\frac{k_{-2} + k_3 - 1/\tau_2}{1/\tau_1 - 1/\tau_2}\exp\left(-\frac{t}{\tau_1}\right) + C\,k_{-2}\frac{k_{-2} + k_3 - 1/\tau_1}{1/\tau_2 - 1/\tau_1}\exp\left(-\frac{t}{\tau_2}\right), \qquad \text{(Equation 5)}$$

where C is constant, and time constants τ_1 and τ_2 are given by

$$\tau_1 = \left\{\frac{1}{2}\left(k_{-2} + k_3 + k_{-3} + \sqrt{(k_{-2} + k_3 + k_{-3})^2 - 4k_{-2}k_{-3}}\right)\right\}^{-1} \qquad \text{(Equation 6)}$$

and

$$\tau_2 = \left\{\frac{1}{2}\left(k_{-2} + k_3 + k_{-3} - \sqrt{(k_{-2} + k_3 + k_{-3})^2 - 4k_{-2}k_{-3}}\right)\right\}^{-1}. \qquad \text{(Equation 7)}$$

Calculation of Kinetic Parameters

Independently of the determination of kinetic parameters using Equation 1, preexponential factors, A_1 and A_2, and time constants, τ_1 and τ_2, can be obtained by calculation from rate constants indicated in Figure 7, as indicated in the right column of Table S1. For Model WT, time constants, τ_1 and τ_2, are described as Equation 3 and Equation 4, respectively, while preexponential factors, A_1 and A_2, are given by

$$A_1 = C\left\{k_{-2} + \left(k_{-2} + k_3 - \frac{1}{\tau_1}\right)\frac{k_4}{k_{-3}}\right\}\frac{k_{-2} + k_3 - 1/\tau_2}{1/\tau_1 - 1/\tau_2} \qquad \text{(Equation 8)}$$

and

$$A_2 = C\left\{k_{-2} + \left(k_{-2} + k_3 - \frac{1}{\tau_2}\right)\frac{k_4}{k_{-3}}\right\}\frac{k_{-2} + k_3 - 1/\tau_1}{1/\tau_2 - 1/\tau_1}. \qquad \text{(Equation 9)}$$

For Model E584Q (rate constant k_4 = 0), time constants, τ_1 and τ_2, are described as Equation 6 and Equation 7, respectively, while preexponential factors, A_1 and A_2, are given by

$$A_1 = C\,k_{-2}\frac{k_{-2}+k_3-1/\tau_2}{1/\tau_1-1/\tau_2} \quad \text{(Equation 10)}$$

and

$$A_2 = C\,k_{-2}\frac{k_{-2}+k_3-1/\tau_1}{1/\tau_2-1/\tau_1}. \quad \text{(Equation 11)}$$

SUPPLEMENTAL INFORMATION

Supplemental Information includes six figures, one table, and four movies and can be found with this article online at http://dx.doi.org/10.1016/j.str.2013.08.017.

ACKNOWLEDGMENTS

We thank A. Miyagi for setting up the high-speed AFM apparatus used in this study, K. Karata for cloning of the human *VCP* gene, T. Uchihashi for simulation of AFM image, K. Namba for advice on image processing, and T. Yamaguchi for suggestions to the presentation in enzymology. We are indebted to A. Förster, X. Zhang, and P. Freemont for stimulating discussion. We also thank members of the Ogura and Ando laboratories for stimulating discussion and suggestions. This work was supported in part by the Core Research for Evolutional Science and Technology (CREST) program grant from the Japan Science and Technology Agency (JST; to T.A. and T.O.); by grants from the Ministry of Education, Culture, Sports, Science and Technology (MEXT) of Japan (19058012, 24370056, 24659432, and 25117517 to T.O.; 24117001a and 24117004a to T.K.; and 20221006 to T.A.); by the program of Joint Usage/Research Center for Developmental Medicine, Institute of Molecular Embryology and Genetics, Kumamoto University (to D.Y.); and by the Global COE Program (Cell Fate Regulation Research and Education Unit) from MEXT, Japan. K.N. and K.-i.A.-M. were research associate and junior research associate, respectively, of the Global COE. T.O. was a Global COE member.

Received: March 20, 2013
Revised: August 19, 2013
Accepted: August 19, 2013
Published: September 19, 2013

REFERENCES

Ammelburg, M., Frickey, T., and Lupas, A.N. (2006). Classification of AAA$^+$ proteins. J. Struct. Biol. *156*, 2–11.

Ando, T., Kodera, N., Takai, E., Maruyama, D., Saito, K., and Toda, A. (2001). A high-speed atomic force microscope for studying biological macromolecules. Proc. Natl. Acad. Sci. USA *98*, 12468–12472.

Ando, T., Uchihashi, T., and Fukuma, T. (2008). High-speed atomic force microscopy for nano-visualization of dynamic biomolecular processes. Prog. Surf. Sci. *83*, 337–437.

Barthelme, D., and Sauer, R.T. (2012). Identification of the Cdc48•20S proteasome as an ancient AAA+ proteolytic machine. Science *337*, 843–846.

Barthelme, D., and Sauer, R.T. (2013). Bipartite determinants mediate an evolutionarily conserved interaction between Cdc48 and the 20S peptidase. Proc. Natl. Acad. Sci. USA *110*, 3327–3332.

Beuron, F., Flynn, T.C., Ma, J., Kondo, H., Zhang, X., and Freemont, P.S. (2003). Motions and negative cooperativity between p97 domains revealed by cryo-electron microscopy and quantised elastic deformational model. J. Mol. Biol. *327*, 619–629.

Briggs, L.C., Baldwin, G.S., Miyata, N., Kondo, H., Zhang, X., and Freemont, P.S. (2008). Analysis of nucleotide binding to P97 reveals the properties of a tandem AAA hexameric ATPase. J. Biol. Chem. *283*, 13745–13752.

Buchberger, A. (2013). Roles of cdc48 in regulated protein degradation in yeast. Subcell. Biochem. *66*, 195–222.

Chan, K.M., Delfert, D., and Junger, K.D. (1986). A direct colorimetric assay for Ca^{2+} -stimulated ATPase activity. Anal. Biochem. *157*, 375–380.

Chang, L.F., Chen, S., Liu, C.C., Pan, X., Jiang, J., Bai, X.C., Xie, X., Wang, H.W., and Sui, S.F. (2012). Structural characterization of full-length NSF and 20S particles. Nat. Struct. Mol. Biol. *19*, 268–275.

Davies, J.M., Tsuruta, H., May, A.P., and Weis, W.I. (2005). Conformational changes of p97 during nucleotide hydrolysis determined by small-angle X-Ray scattering. Structure *13*, 183–195.

Davies, J.M., Brunger, A.T., and Weis, W.I. (2008). Improved structures of full-length p97, an AAA ATPase: implications for mechanisms of nucleotide-dependent conformational change. Structure *16*, 715–726.

DeLaBarre, B., and Brunger, A.T. (2003). Complete structure of p97/valosin-containing protein reveals communication between nucleotide domains. Nat. Struct. Biol. *10*, 856–863.

DeLaBarre, B., Christianson, J.C., Kopito, R.R., and Brunger, A.T. (2006). Central pore residues mediate the p97/VCP activity required for ERAD. Mol. Cell *22*, 451–462.

Esaki, M., and Ogura, T. (2010). ATP-bound form of the D1 AAA domain inhibits an essential function of Cdc48p/p97. Biochem. Cell Biol. *88*, 109–117.

Forouzan, D., Ammelburg, M., Hobel, C.F., Ströh, L.J., Sessler, N., Martin, J., and Lupas, A.N. (2012). The archaeal proteasome is regulated by a network of AAA ATPases. J. Biol. Chem. *287*, 39254–39262.

Hanson, P.I., and Whiteheart, S.W. (2005). AAA+ proteins: have engine, will work. Nat. Rev. Mol. Cell Biol. *6*, 519–529.

Huyton, T., Pye, V.E., Briggs, L.C., Flynn, T.C., Beuron, F., Kondo, H., Ma, J., Zhang, X., and Freemont, P.S. (2003). The crystal structure of murine p97/VCP at 3.6A. J. Struct. Biol. *144*, 337–348.

Igarashi, K., Uchihashi, T., Koivula, A., Wada, M., Kimura, S., Okamoto, T., Penttilä, M., Ando, T., and Samejima, M. (2011). Traffic jams reduce hydrolytic efficiency of cellulase on cellulose surface. Science *333*, 1279–1282.

Johnson, J.O., Mandrioli, J., Benatar, M., Abramzon, Y., Van Deerlin, V.M., Trojanowski, J.Q., Gibbs, J.R., Brunetti, M., Gronka, S., Wuu, J., et al.; ITALSGEN Consortium. (2010). Exome sequencing reveals *VCP* mutations as a cause of familial ALS. Neuron *68*, 857–864.

Kodera, N., Yamamoto, D., Ishikawa, R., and Ando, T. (2010). Video imaging of walking myosin V by high-speed atomic force microscopy. Nature *468*, 72–76.

Lupas, A.N., and Martin, J. (2002). AAA proteins. Curr. Opin. Struct. Biol. *12*, 746–753.

Meyer, H., Bug, M., and Bremer, S. (2012). Emerging functions of the VCP/p97 AAA-ATPase in the ubiquitin system. Nat. Cell Biol. *14*, 117–123.

Nishikori, S., Esaki, M., Yamanaka, K., Sugimoto, S., and Ogura, T. (2011). Positive cooperativity of the p97 AAA ATPase is critical for essential functions. J. Biol. Chem. *286*, 15815–15820.

Ogura, T., and Wilkinson, A.J. (2001). AAA$^+$ superfamily ATPases: common structure—diverse function. Genes Cells *6*, 575–597.

Pye, V.E., Dreveny, I., Briggs, L.C., Sands, C., Beuron, F., Zhang, X., and Freemont, P.S. (2006). Going through the motions: the ATPase cycle of p97. J. Struct. Biol. *156*, 12–28.

Rodriguez, T.R., and Garcia, R. (2003). Theory of Q control in atomic force microscopy. Appl. Phys. Lett. *82*, 4821–4823.

Rouiller, I., Butel, V.M., Latterich, M., Milligan, R.A., and Wilson-Kubalek, E.M. (2000). A major conformational change in p97 AAA ATPase upon ATP binding. Mol. Cell *6*, 1485–1490.

Rouiller, I., DeLaBarre, B., May, A.P., Weis, W.I., Brunger, A.T., Milligan, R.A., and Wilson-Kubalek, E.M. (2002). Conformational changes of the multifunction p97 AAA ATPase during its ATPase cycle. Nat. Struct. Biol. *9*, 950–957.

Satapathy, A.K., and Richardson, C.C. (2011). The glutamate switch of bacteriophage T7 DNA helicase: role in coupling nucleotide triphosphate (NTP) and DNA binding to NTP hydrolysis. J. Biol. Chem. *286*, 23113–23120.

Song, C., Wang, Q., and Li, C.C. (2003). ATPase activity of p97-valosin-containing protein (VCP). D2 mediates the major enzyme activity, and D1 contributes to the heat-induced activity. J. Biol. Chem. *278*, 3648–3655.

Stolz, A., Hilt, W., Buchberger, A., and Wolf, D.H. (2011). Cdc48: a power machine in protein degradation. Trends Biochem. Sci. *36*, 515–523.

Uchihashi, T., Iino, R., Ando, T., and Noji, H. (2011). High-speed atomic force microscopy reveals rotary catalysis of rotorless F_1-ATPase. Science *333*, 755–758.

Watts, G.D., Wymer, J., Kovach, M.J., Mehta, S.G., Mumm, S., Darvish, D., Pestronk, A., Whyte, M.P., and Kimonis, V.E. (2004). Inclusion body myopathy associated with Paget disease of bone and frontotemporal dementia is caused by mutant valosin-containing protein. Nat. Genet. *36*, 377–381.

Weihl, C.C., Pestronk, A., and Kimonis, V.E. (2009). Valosin-containing protein disease: inclusion body myopathy with Paget's disease of the bone and frontotemporal dementia. Neuromuscul. Disord. *19*, 308–315.

Wendel, M., Lorenz, H., and Kotthaus, J.P. (1995). Sharpened electron beam deposited tips for high resolution atomic force microscope lithography and imaging. Appl. Phys. Lett. *67*, 3732–3734.

Yamamoto, D., Nagura, N., Omote, S., Taniguchi, M., and Ando, T. (2009). Streptavidin 2D crystal substrates for visualizing biomolecular processes by atomic force microscopy. Biophys. J. *97*, 2358–2367.

Yamanaka, K., Sasagawa, Y., and Ogura, T. (2012). Recent advances in p97/VCP/Cdc48 cellular functions. Biochim. Biophys. Acta *1823*, 130–137.

Zhang, X., and Wigley, D.B. (2008). The 'glutamate switch' provides a link between ATPase activity and ligand binding in AAA+ proteins. Nat. Struct. Mol. Biol. *15*, 1223–1227.

Zhang, X., Shaw, A., Bates, P.A., Newman, R.H., Gowen, B., Orlova, E., Gorman, M.A., Kondo, H., Dokurno, P., Lally, J., et al. (2000). Structure of the AAA ATPase p97. Mol. Cell *6*, 1473–1484.

